THE JOURNAL OF PHYSICAL CHEMISTRY C

pubs.acs.org/JPCC Article

Inducing Superparamagnetism and High Magnetization in Nickel Cobaltite ($Ni_xCo_{3-x}O_4$) Spinel Nanoparticles by Controlling Ni Mole Fraction and Cation Distribution

Jesús Alberto Ramos Ramón, Jose Luis Ortiz-Quiñonez, Apurba Ray, Sachindranath Das, and Umapada Pal*

Cite This: *J. Phys. Chem. C* 2020, 124, 18264−18274 Read Online

ACCESS | Metrics & More | Article Recommendations | Supporting Information

ABSTRACT: Recently Ni−Co mixed oxide nanoparticles have received tremendous attention for their application potential in electrochemical devices, biosensing, and biomedical treatments. However, the biomedical application of these nanostructures is severely restricted due to their poor magnetic properties. Here we present the fabrication of nickel cobaltite nanoparticles of 17−40 nm size range with different Ni contents by a simple glycol-mediated sol−gel process. We demonstrate that, by controlling Ni content in the mixed oxide nanoparticles, their lattice structure can be transformed from inverse spinel to partially inverse spinel lattice. Moreover, by controlling the site occupancy of $Co^{2+,3+}$ and $Ni^{2+,3+}$ ions, their net magnetization can be enhanced substantially. The nanoparticles prepared with a nickel/cobalt ratio of 0.25 manifest superparamagnetic behavior with room temperature saturation magnetization as high as 66.3 emu/g (2.75 μ_B) and coercivity as low as 85 Oe, which indicate their great potential for biomedical applications such as hyperthermia and targeted drug delivery.

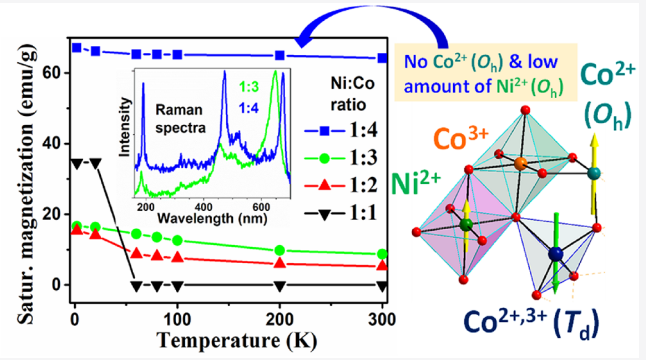

1. INTRODUCTION

Nickel cobaltite ($NiCo_2O_4$) is a multifunctional semiconductor which has received ample research attention in recent times. In nanostructure form, it has been utilized in electrochemical devices, such as electrodes in supercapacitors,[1,2] anodes for electrocatalytic oxygen evolution reactions,[3] and electrochemical immunosensing.[4] $NiCo_2O_4$ nanoparticles (NPs) have also been tested for biological and biomedical applications.[5] Apart from their easy functionalization, these NPs are stable in water (negligible leaching of Ni or Co ions), form conjugates with amino acids and drugs, and exhibit low toxicity to different cells.[5] On the other hand, magnetic properties of Ni−Co-based oxides have been the subject of intense scientific research due to their potential applications in spintronics, exploiting their intrinsic ferrimagnetic order and metallic electrical behavior.[6] However, understanding the magnetic behavior of $NiCo_2O_4$ remained unclear due to contradicting results published in the literature,[7−17] especially on its saturation magnetization (M_s) values. The reported M_s values per formula unit of $NiCo_2O_4$ vary from ∼6.25 emu/g (0.26 μ_B) to ∼38.0 emu/g (1.58 μ_B). In some cases, the room temperature M_s value is inexplicably low (∼2 emu/g or 0.086 μ_B).[10,13−15] Also, there is no consensus whether all the Ni cations are located at octahedral sites (O_h) of $NiCo_2O_4$ spinel.[16] The reason for such a discrepancy probably lies in the presence of impurities (such as NiO, $Ni_xCo_{1-x}O_y$, α/β-$Ni(OH)_2$, α/β-$Co(OH)_2$, Co_3O_4, cobalt carbonates, etc.) in varied amounts, which also affect the technological application of $NiCo_2O_4$ spinel such as in a supercapacitor and lithium ion battery (LIB).[18−20] While a direct identification of cation locations in spinel lattice is almost impossible, a detailed magnetic characterization can shed enough light on the distribution of multivalent cations at different lattice sites. On the other hand, while the magnetic properties of other ferrites such as $CoFe_2O_4$ and $BiFeO_3$ of spinel and distorted-perovskite structures have been studied extensively to understand cation coordination in their lattices,[21,22] there does not exist enough information in the literature on $Ni_xCo_{3-x}O_4$ spinel.

Moreover, use of a great variety of synthesis methods with distinct synthesis conditions and after-growth thermal treatments made it difficult to establish a direct relationship

Received: April 6, 2020
Revised: July 27, 2020
Published: July 29, 2020

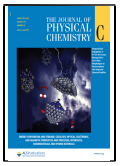

https://dx.doi.org/10.1021/acs.jpcc.0c03075
J. Phys. Chem. C 2020, 124, 18264−18274

between the cation distribution and physicochemical properties of $NiCo_2O_4$ nanostructures. In general, the compounds of AB_2O_4 stoichiometry, such as $NiCo_2O_4$, have an inverse spinel type crystal structure, where A and B are doubly and triply charged cations, respectively. In an ideal inverse spinel type structure, while B cations are equally distributed in tetrahedral (T_d) and octahedral (O_h) sites, the A cations occupy only the octahedral sites. Although it has been well-established that physical properties of $NiCo_2O_4$ are governed by cation accommodation sequence in its lattice,[23] depending on the synthesis technique and utilized precursors therein,[24] distribution of cations and their oxidation states in inverse spinel structures can be different, even for compounds of the same composition. While several efforts have been made to understand this process, the majority of the analyses have been carried out for $NiCo_2O_4$, i.e., for a fixed Ni mole fraction ($x = 1$ in $Ni_xCo_{3-x}O_4$), without taking into consideration the effect of the Ni mole fraction on the cation distribution in the inverse spinel lattice. Therefore, a study on the effect of cation accommodation and their valence states on the magnetic properties in Ni−Co mixed oxides nanostructures, where the oxidation states of Ni and Co ions can be either 2+ or 3+, is necessary for varied molar fractions of Ni, to shed light on their physical properties.

In this work, we present the fabrication of Ni−Co mixed oxide nanoparticles of different Ni:Co molar ratios by a simple glycol-mediated sol−gel process. Effects of the Ni mole fraction on the structural, vibrational, and magnetic properties of the mixed oxide nanostructures have been studied using X-ray diffraction (XRD), room temperature Raman and Fourier transform infrared (FTIR) spectroscopies, and vibrating sample magnetometry (VSM) in the 1.8−300 K temperature range. Effect of the nickel fraction on the cation coordination and its consequence on the magnetic behavior of the inverse spinel nanostructures have been analyzed and discussed extensively.

2. EXPERIMENTAL SECTION

Chemicals and Solvents. Nickel acetate tetrahydrate ($Ni(CH_3COO)_2{\cdot}4H_2O$, LobaChemie, 98.0%), cobalt(II) acetate tetrahydrate ($Co(CH_3COO)_2{\cdot}4H_2O$, LobaChemie, 99%), polyvinylpyrrolidone (PVP, M_W 40 000, Sigma-Aldrich), ethylene glycol ($C_2H_6O_2$, EG, Merck, 99.0%), and ethanol (Merck, 99.9%) were utilized for the experiments. All the chemicals were of analytical grade and were used without further purification. Deionized (DI) water from a Milli-Q system (ρ > 18.2 M Ω·cm) was utilized for washing the synthesized nanostructures and glassware.

Fabrication of Ni−Co Mixed Oxide Nanoparticles. For the synthesis of Ni−Co mixed oxide nanoparticles of different Ni:Co molar ratios (1:1, 1:2, 1:3, and 1:4), nickel acetate and cobalt acetate in appropriate molar ratios were dissolved in 70 mL of EG under magnetic stirring for 10 min. About 0.15 g of PVP was then added to the solution and kept under continuous magnetic stirring for another 50 min to obtain a homogeneous transparent solution. After that, the solution was heated to 180 °C in an open-air oven for 4 h and then cooled to room temperature. The precipitate formed at the bottom of the reaction flask was collected by centrifugation (12 000 rpm, 20 min), washed several times with ethanol and DI water, and dried at 150 °C for 48 h. The obtained powder was air-annealed at 400 °C for 2 h in a muffle furnace, increasing the temperature at 2 °C/min.

Characterization of Ni−Co Mixed Oxide Nanoparticles. For morphology and composition analysis of the synthesized nanostructures, a small amount of each of the powder samples was dispersed in ethanol and deposited over a clean Si wafer. The samples were inspected in a JEOL JSM-7800F field-emission scanning electron microscope (FE-SEM) coupled with an Oxford Instrument X-Max spectrometer. A Rigaku MiniFlex 600 benchtop diffractometer with Cu Kα radiation source (λ = 1.5406 Å) operating at 40 kV and 40 mA was utilized to record the X-ray diffraction (XRD) patterns of the powder samples to determine their crystallinity and structural phase. For the analysis of vibrational properties of the mixed oxide nanostructures, their Fourier transform infrared (FTIR) spectra were recorded at room temperature in 400−4000 cm^{-1} spectral range in a PerkinElmer FTIR Spectrum RX1 spectrometer. For FTIR analysis, the powder samples were cold pressed to form thin pellets of 13 mm diameter by mixing about 1 mg of each sample with 99 mg of dry KBr. Crystalline quality and associated defects in the nanostructures were analyzed further by Raman spectroscopy at room temperature. A Horiba Lab RAM HR system equipped with a 633 nm He−Ne laser and a thermoelectrically cooled charge-coupled device (CCD) detector were utilized for recording Raman spectra of the samples. The effect of the Ni content on the magnetic behaviors of the fabricated nanostructures was studied in a DynaCool-9 (Quantum Design) physical property measurement system (PPMS). Magnetization hysteresis ($M-H$) loops of the samples were recorded at different temperatures (1.8, 20, 60, 80, 100, 200, and 300 K) under ±5.0 T applied magnetic field. Temperature-dependent magnetization curves of the samples were recorded in 1.8−300 K temperature range under a constant magnetic field of 100 Oe.

3. RESULTS AND DISCUSSION

Figure 1 presents typical SEM images of the Ni−Co mixed oxide nanostructures fabricated at different nominal mole fractions of Ni. As can be noticed, all the samples contain agglomerated quasi-spherical particles of 17−40 nm size range. While a similar agglomeration behavior of nanoparticles can be seen for all the samples, the nanoparticles in the sample prepared with a Ni:Co molar ratio of 1:1 (Figure 1a) are larger than the nanoparticles in other samples. Energy dispersive spectra (EDS) of the nanostructures revealed emission bands associated with Ni, Co, O, and C (Figure 1e,f). While the Ni:Co atomic ratios estimated from EDS analysis of the samples remained close to their nominal values (Table 1), detection of C in high atomic percentage in the samples indicates the presence of organic molecules at the surface of the nanostructures. It should be remembered that the samples for EDS analysis were prepared over clean silicon wafers instead of carbon tape commonly utilized for SEM analysis of powder samples. The probable origin of C in the samples is the formation of metal carbonates during thermal annealing. Although the samples were annealed in air, the carbonate compounds did not dissociate completely at such a low temperature (400 °C). The adapted process of sample preparation might also be responsible for detection of high carbon content in their EDS analysis. We used ethanol as the dispersing medium of the nanostructures to prepare the samples for SEM−EDS analysis. The surface adsorbed ethanol might also be a source of carbon, as ethanol gets pyrolyzed by the exposure of a high-energy electron beam inside the high

https://dx.doi.org/10.1021/acs.jpcc.0c03075
J. Phys. Chem. C 2020, 124, 18264−18274

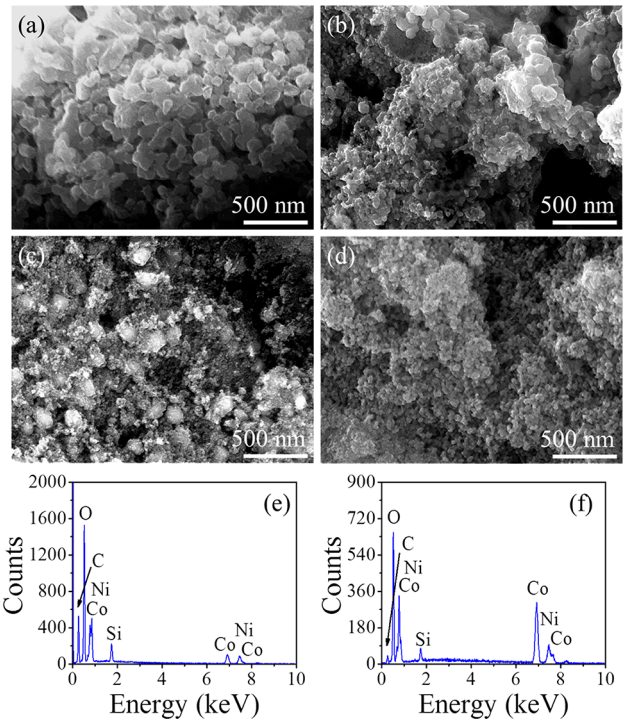

Figure 1. Typical SEM images of Ni−Co mixed oxide nanoparticles prepared at nominal Ni:Co molar ratios: (a) 1:1, (b) 1:2, (c) 1:3, and (d) 1:4. Typical EDS spectra of the nanostructures containing (e) highest (Ni:Co = 1:1) and (f) lowest (Ni:Co = 1:4) Ni fractions.

vacuum microscope chamber. As can be noticed in Table 1, the carbon content in the samples varied between 43 and 25 atom % with no specific trend, clearly indicating the contribution of an uncontrolled source such as ethanol used for dispersing the nanostructures.

XRD patterns of the mixed oxide nanostructures with different Ni contents (Figure 2) revealed intense and well-defined diffraction peaks correspond to the cubic spinel structure of $NiCo_2O_4$ (JCPDS No. 20-0781).[25,26] The diffraction peaks appearing around 2θ = 30.96, 36.53, 44.25, 55.57, 59.17, and 64.92° correspond to the (220), (311), (400), (422), (511), and (440) planes, respectively. Two additional peaks around 42.92 and 62.34° appeared for the samples prepared at Ni:Co molar ratios of 1:2 and 1:3, which correspond to the NaCl-type cubic structure of $Ni_{1-x}Co_xO$.[27] The (111) plane of $Ni_{1-x}Co_xO$ overlapped with the (311) plane of the $Ni_xCo_{3-x}O_4$ spinel. The remaining (311) and (222) planes of $Ni_{1-x}Co_xO$ were not observed due to their very low relative intensity. Since both NiO and CoO have NaCl-type cubic structure, and Ni^{2+} and Co^{2+} cations have similar ionic radii, formation of the $Ni_{1-x}Co_xO$ byproduct in the samples is quite reasonable. However, additional diffraction

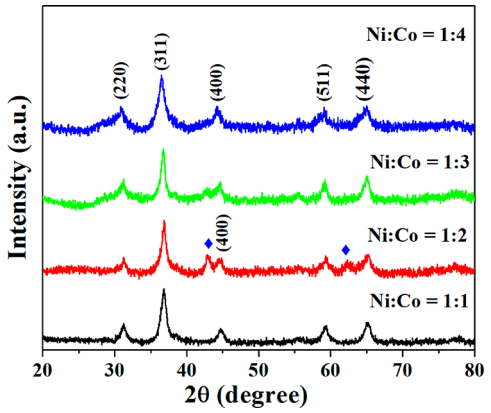

Figure 2. XRD spectra of $Ni_xCo_{3-x}O_4$ nanoparticles of cubic spinel structure prepared at different Ni:Co molar ratios. Blue diamond symbols indicate peaks corresponding to $Ni_{1-x}Co_xO$ impurity of cubic NaCl-type structure.

peaks associated with any other secondary phase, such as NiO, were not detected.

As the positions of the diffraction peaks and lattice parameter value (8.084 Å) of Co_3O_4 spinel are very close to the corresponding values of $Ni_xCo_{3-x}O_4$ (Figure 2 and Table 2), we included the XRD pattern of Co_3O_4 NPs synthesized by the same synthesis process in Figure S1. As can be seen, while the positions of the peaks revealed in the XRD patterns of Co_3O_4 and $Ni_xCo_{3-x}O_4$ samples are pretty close, they are almost the same for the samples having Ni:Co ratios of 1:1 and 1:2. However, as has been discussed later, no evidence of Co_3O_4 formation was found in the Raman spectra of these samples. The appearance of relatively broad diffraction peaks indicates the nanocrystalline nature of the powder samples.[28,29] Furthermore, on increase of the Ni fraction, the position of all the diffraction peaks shifted toward higher angles indicating a minor lattice shrinkage caused by the replacement of Co atoms of octahedral (O_h) sites of the spinel lattice by Ni atoms. This makes sense since the reported Shannon ionic radii for Ni^{2+} and Co^{2+} at high spin at O_h sites are 0.69 and 0.745 Å, respectively (see Table S1). Estimated lattice parameters of the fabricated mixed oxide nanocrystal are presented in Table 2.

Table 2. XRD Estimated Lattice Parameter Values for Ni−Co Mixed Oxide Nanoparticles Prepared with Different Nominal Ni Mole Fractions (x)

nominal Ni:Co molar ratio	lattice parameter (Å)
1:1	8.087
1:2	8.075
1:3	8.103
1:4	8.153

Table 1. EDS Estimated Elemental Composition of Ni−Co Mixed Oxide Nanoparticles Prepared at Different Ni:Co Molar Ratios[a]

nominal Ni:Co molar ratio	C (atom %)	Co (atom %)	Ni (atom %)	O (atom %)	Ni/Co atomic ratio
1:1	42.92	3.86	3.93	49.30	1.02
1:2	29.27	15.26	7.55	47.92	0.50
1:3	11.32	29.97	9.64	49.06	0.33
1:4	25.13	20.67	6.13	48.07	0.28

[a]Presented compositions are the average of compositions estimated at least five different places of each of the samples.

https://dx.doi.org/10.1021/acs.jpcc.0c03075
J. Phys. Chem. C 2020, 124, 18264−18274

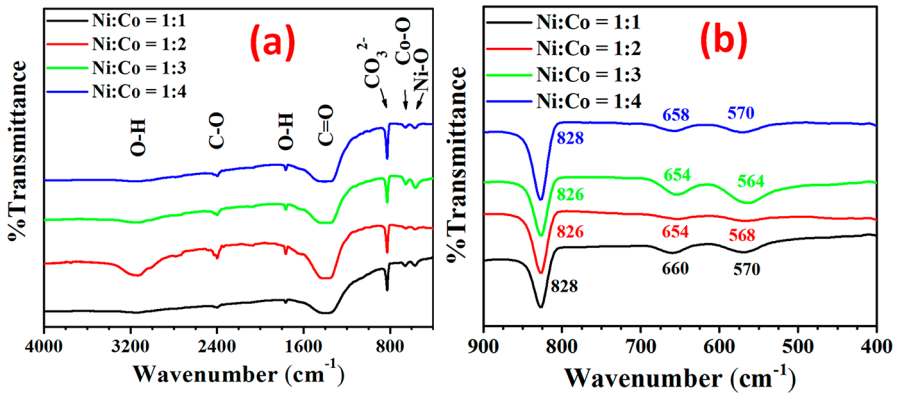

Figure 3. FTIR spectra (a) of Ni−Co mixed oxide nanoparticles containing different Ni molar fractions. An amplified low frequency region has been presented in (b) for a better visibility of the low intensity peaks.

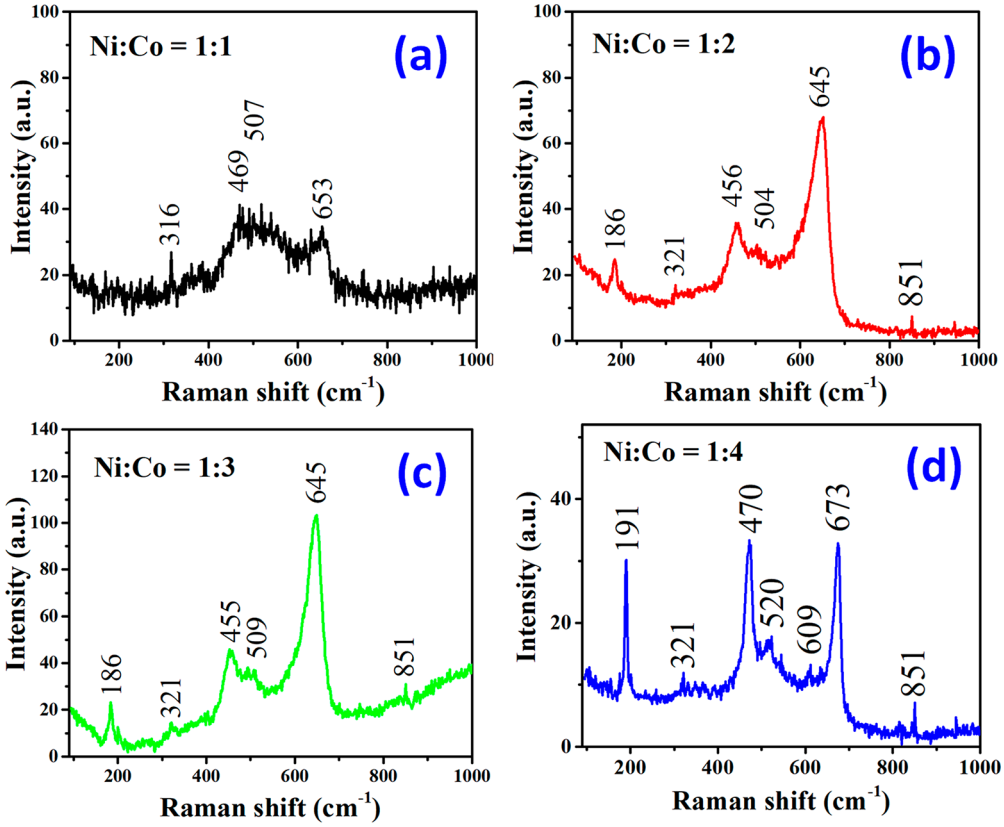

Figure 4. Room temperature Raman spectra of Ni−Co oxide nanoparticles containing different Ni:Co molar ratios.

The lattice parameter values of the nanocrystals increased marginally with the decrease of the Ni fraction, and they are very close to the lattice parameter values of $NiCo_2O_4$ nanostructures (Ni:Co = 1:2) reported in the literature.[24,30]

The Ni−Co mixed oxides with Ni:Co molar ratios of 1:1, 1:2, 1:3, and 1:4 can also be expressed as $Ni_{0.5}Co_{0.5}O_y$, $Ni_{0.33}Co_{0.67}O_y$, $Ni_{0.25}Co_{0.75}O_y$, and $Ni_{0.20}Co_{0.80}O_y$, respectively. As has been observed by Windisch et al.,[23] the lattice structure of $Ni_{1-x}Co_xO_y$ systematically changes from spinel type (x = 1.0) to inverse spinel type ($0.67 > x > 0.25$) through a multiphase transition region. Room temperature FTIR spectra of the mixed oxide nanoparticles of different Ni contents are presented in Figure 3. The sharp absorption band appearing around 1766 cm^{-1} and the broad absorption band appearing between 3000 and 3380 cm^{-1} can be assigned to the bending and stretching modes of O−H originated from water, physisorbed over the sample surface. The absorption band centered around 2397 cm^{-1} can be associated with the characteristic ν(C−H) stretching mode,[31,32] probably appearing from the unreacted metal precursors or the ethylene glycol utilized in the synthesis process. The broad absorption band appearing between 1300 and 1540 cm^{-1} can be attributed to $\nu(COO^-)$ groups of the metal acetate precursors.[33] The sharp absorption band revealed around 826.9 cm^{-1} for all the samples could be from cobalt and/or nickel carbonates generated by the reaction of metal precursors with organic residue of ethylene glycol or PVP. Vibrational bands of carbonates containing Co(III) ions have been reported to appear in the 821−850 and 1260−1480 cm^{-1} spectral ranges.[34]

https://dx.doi.org/10.1021/acs.jpcc.0c03075
J. Phys. Chem. C 2020, 124, 18264−18274

Table 3. Position and Assignation of Vibrational Modes Revealed in Raman Spectra of Ni−Co Mixed Oxide Nanoparticles

nominal Ni:Co molar ratio	F_{2g}	β-Ni(OH)$_2$	E_g	F_{2g}	F_{2g}	A_{1g}	wavelength of exciting laser (nm)	ref
1:1	–	316	469	–	–	653	633	this work
1:2	185	321	456	504	–	645	633	this work
1:3	186	321	455	509	–	645	633	this work
1:4	191	321	470	520	609	673	633	this work
1:2	186		460	505		659	633	14
1:2	186		469	519		668	–	49
1:2	186		477	523		671	532	13
1:2	187		480	523	592	668	488	7[a]
1:2	199		484	527	610	682	488	7[b]
1:4	–	–	478	–	–	674	488	23

[a]$NiCo_2O_4$ thin films grown over $MgAl_2O_4(001)$ substrates at temperature (T_{sub}) 250 °C. [b]$NiCo_2O_4$ thin films grown over $MgAl_2O_4(001)$ substrates at temperature (T_{sub}) 550 °C.

All the samples revealed two low-intensity peaks around 568 and 657 cm^{-1}, which are the most significant characteristic peaks associated with the stretching vibrations of the Ni−O and Co−O bonds in mixed oxide,[35,36] respectively. It can be recalled that the presence of organic precursors in the fabricated nanostructures was also evident in their EDS spectra (Figure 1e,f), which revealed intense C emissions. As has been mentioned earlier, all the nanostructures were air-annealed at 400 °C prior to their characterization. Considering a temperature as high as 500 °C is required to remove the carbon fully from metal oxide nanostructures,[37] the annealing temperature utilized in this work is considerably low. However, the low stability of the inverse spinel nanostructures at temperatures higher than 400 °C makes it impossible to apply higher annealing temperature, avoiding the formation of undesired secondary phases, such as NiO or Co_3O_4.[6] An air annealing above 450 °C has been seen to affect the usual magnetic and electrical behaviors of $NiCo_2O_4$ drastically. As has been reported by Dileep et al., $NiCo_2O_4$ thin films annealed above 450 °C present nonmagnetic and insulating behaviors.[38]

As can be seen in Figure 3b, the intensity ratio of the 826 cm^{-1} (associated with carbonate impurity) and 654 cm^{-1}(associated with $Ni_xCo_{3-x}O_4$ spinel) IR bands (I_{826}/I_{654}) is pretty high for the samples with Ni:Co ratios of 1:2 and 1:4, indicating high carbonate impurity content in them. The I_{826}/I_{654} ratios (estimated from Figure 3b) for the samples with Ni:Co = 1:1, 1:2, 1:3 and 1:4 were ∼7, 16, 5, and 12, respectively.

Room temperature Raman spectra of the mixed oxide nanostructures were recorded in the 90−1000 cm^{-1} spectral range to observe the effect of the Ni fraction on their vibrational properties (Figure 4). The Raman spectrum of the sample with the lowest Ni content (Ni:Co = 1:4) revealed three well-defined vibrational modes around 191 (F_{2g}), 470 (E_g), and 673 cm^{-1} (A_{1g}), along with two low-intensity modes around 520 (F_{2g}) and 609 cm^{-1} (F_{2g}). Positions of the principal vibrational modes revealed in the samples prepared at different Ni:Co molar ratios along with their probable assignments are presented in Table 3. Although the Co and Ni ions have similar masses, incorporation of Ni has a strong effect on the vibrational and structural properties of Ni−Co mixed oxide nanocrystals. Observed differences in the positions of the vibration modes for the samples containing different Ni contents could be associated with the size difference between Co^{2+} and Ni^{2+} cations (the Co^{2+} cation is ∼7% larger than the Ni^{2+} cation) when both of them occupy O_h sites[39] and the structural transformation of the lattice from inverse spinel to partially inverse spinel, as discussed later. The low-intensity narrow band appearing at 321 cm^{-1} (or 316 cm^{-1}) corresponds to the E_g lattice mode of β-Ni(OH)$_2$.[40−42]

In addition, the crystal field stabilization energies (CFSEs) for the Co^{2+} and Ni^{2+} cations at O_h sites are 88 and 122 kJ/mol, respectively,[43] while their CFSEs at T_d sites are 58.7 and 36.2 kJ/mol, respectively. These values suggest the Ni^{2+} cations have a higher tendency to occupy O_h sites than Co^{2+} cations.[43] In fact, from the difference between the CFSE values for octahedral and tetrahedral sites, Zhao et al. estimated the octahedral site preference energies (OSPEs) of $Co^{2+,3+}$ and Ni^{2+} ions (Table 4).[44] A higher absolute OSPE value for a cation suggests its preference for occupying the octahedral site (O_h).[44] According to Liu et al., the OSPE values of these divalent and trivalent cations in the spinel structure follow the order $Co^{2+} < Ni^{3+} < Co^{3+} < Ni^{2+}$,[45] and consequently, Ni^{2+} must be located at O_h sites and Co^{2+} must be located at T_d sites of the $Ni_xCo_{3-x}O_4$ spinel lattice.[45] Considering that the OSPE value for Co^{3+} is higher than that of Co^{2+} but lower than that of Ni^{2+}, Co^{3+} ions are expected to be located at both O_h and T_d sites. In the specific case of $NiCo_2O_4$, using X-ray absorption spectroscopy, Marco et al. confirmed that the Ni^{2+} ions are located at O_h sites and Co^{3+} ions are located both at O_h and T_d sites of the spinel lattice.[24] In $Ni_xCo_{3-x}O_4$ spinels with $x < 1$, the presence of Co^{2+} ions is also necessary to maintain the charge neutrality of their lattices. According to Table 4, the Co^{2+} ions prefer to occupy T_d sites rather than O_h sites. Therefore, a partially inverse spinel lattice is obtained for the $Ni_xCo_{3-x}O_4$ nanostructures prepared with Ni:Co = 1:4 molar ratio.

Table 4. Number of d Electrons, Crystal Field Stabilization Energy (CFSE), and Octahedral Site Preference Energy (OSPE) of $Co^{2+,3+}$ and Ni^{2+} Ions[44]

ion	no. 3d electrons	CFSE (kJ mol^{-1}) octahedral site	CFSE (kJ mol^{-1}) tetrahedral site	OSPE (kJ mol^{-1})
Co^{2+}	7	−92.9	−61.9	−31.0
Co^{3+}	6	−188.3	−108.8	−79.5
Ni^{2+}	8	−122.2	−36.0	−86.2

In general, with the increase of Ni content, the Raman dispersion bands of the mixed oxide become broader, indicating a loss of symmetry caused by local deformation of the spinel lattice. Incorporated Ni ions in cobaltite crystal

https://dx.doi.org/10.1021/acs.jpcc.0c03075
J. Phys. Chem. C 2020, 124, 18264−18274

Table 5. Estimated and Experimental Net Magnetic Moments (in Bohr Magnetons, μ_B) per Formula Unit for Ni−Co Oxide Nanoparticles with Different Nominal Ni:Co Molar Ratios

Ni:Co molar ratio	λ[a]	proposed cation distributions in spinel[b]	estd effective magnetic moment[c,d,e] (μ_{eff})	exptl magnetic moment[f]
1:1	*0.5*	$Co^{2+}_{0.5}Ni^{3+}_{0.5}[Ni^{2+}_{0.5}Ni^{3+}_{0.5}Co^{3+}]O_4$	*0.5·4.53 + 0.5·4.53 − 0.5·3.25 − 0.5·1.9 =* ***1.96***	*1.94*
1:1	1	$Co^{3+}[Ni^{2+}Ni^{3+}_{0.5}Co^{3+}_{0.5}]O_4$	1·5.03 − 1·3.25 − 0.5·1.9 = 0.83	1.94
1:1	1	$Co^{3+}_{0.5}Ni^{3+}_{0.5}[Ni^{2+}Co^{3+}]O_4$	0.5·5.03 + 0.5·4.53 − 1·3.25 = **1.53**	1.94
1:1	0.8	$Co^{3+}_{0.8}Ni^{3+}_{0.2}[Ni^{2+}Ni^{3+}_{0.3}Co^{3+}_{0.7}]O_4$	0.8·5.03 + 0.2·4.53 − 1·3.25 − 0.3·1.9 = **1.11**	1.94
1:2	*1*	$Co^{3+}[Ni^{2+}Co^{3+}]O_4$	*1·5.03 − 1·3.25 =* ***1.78***	*0.848*
1:2	0.65	$Co^{3+}_{0.65}Co^{2+}_{0.35}[Ni^{2+}_{0.65}Ni^{3+}_{0.35}Co^{3+}]O_4$	0.65·5.03 + 0.35·4.53 − 0.65·3.25 − 0.35·1.9 = **2.08**	0.848
1:3	*1*	$Co^{3+}[Ni^{2+}_{0.75}Co^{2+}_{0.25}Co^{3+}]O_4$	*1·5.03 − 0.75·3.25 − 0.25·5.0 =* ***1.34***	*0.865*
1:3	0.75	$Co^{3+}_{0.75}Co^{2+}_{0.25}[Ni^{2+}_{0.75}Co^{3+}_{1.25}]O_4$	0.75·5.03 + 0.25·4.53 − 0.75·3.25= **2.47**	0.865
1:4	1	$Co^{3+}[Ni^{2+}_{0.6}Co^{2+}_{0.4}Co^{3+}]O_4$	1·5.03 − 0.6·3.25 − 0.4·5.0 = **1.08**	2.96
1:4	0.7	$Co^{3+}_{0.7}Co^{2+}_{0.3}[Ni^{2+}_{0.6}Co^{2+}_{0.1}Co^{3+}_{1.3}]O_4$	0.7·5.03 + 0.3·4.53 − 0.6·3.25 − 0.1·5.0 = **2.43**	2.96
1:4	*0.6*	$Co^{3+}_{0.6}Co^{2+}_{0.4}[Ni^{2+}_{0.6}Co^{3+}_{1.4}]O_4$	*0.6·5.03 + 0.4·4.53 − 0.6·3.25 =* ***2.88***	*2.96*

[a] λ = degree of inversion of the spinel. [b] Cations outside and inside the brackets correspond to cations in tetrahedral (T_d) and octahedral (O_h) sites, respectively. [c] Cations in T_d and O_h sites have spin up and spin down, respectively. Therefore, the magnetic moments associated with cations on O_h sites have the minus sign in this column. [d] Effective magnetic moments (μ_{eff}) for $Co^{2+,3+}$ and $Ni^{2+,3+}$ ions in tetrahedral and octahedral sites (Table S1). [e] Values obtained assuming the $t_{2g}^6e_g^0$ configuration for the Co^{3+} ion located at O_h sites.[51] [f] Net magnetic moments obtained from the M_s values (Figure 5) of the samples at T = 1.8 K.

lattice can replace Co ions from O_h sites.[23] In fact, Co_3O_4 (parent crystal structure) has a direct spinel type crystal structure, with $Co^{2+}\{Co^{3+}\}_2\{O^{2-}\}_4$ stoichiometry. While Co^{2+} ions occupy tetrahedral lattice sites (T_d), the Co^{3+} ions remain in octahedral (O_h) sites. Typically, Co_3O_4 manifests five Raman bands around 194, 482, 522, 618, and 691 cm^{-1}, associated with F_{2g}, E_{1g}, F_{2g}, F_{2g}, and A_{1g} vibrational modes, respectively.[14,46]

As can be observed in Figure 4, on change of the Ni:Co ratio from 1:4 to 1:3 or 1:2, the A_{1g} vibrational mode shifts toward lower energy (from ∼673 to ∼645 cm^{-1}) and the band gets significantly broader. This difference suggests that, for Ni:Co = 1:4 ratio, the spinel structure has a certain degree of direct spinel ($0 < \lambda < 0.9$), whereas for other Ni:Co ratios (1:2 and 1:3) the structure is inverse spinel ($\lambda = 1$) (Table 5).[8] λ represents the degree of inversion of the spinel structure, with values 0 and 1 for direct and inverse spinels, respectively. As has been reported by Kumar et al.,[16] the ∼645 cm^{-1} Raman band (A_{1g} mode) shifts toward a higher wavenumber when the spinel lattice transforms from inverse to partially inverse or normal spinel.[16] Since this A_{1g} mode is the characteristic vibrational mode of CoO_6 octahedron units, it can be utilized to monitor the effect of Ni incorporation in the Co_3O_4 crystal lattice.

While the position of the fundamental vibration modes of the spinel nanostructures changes with Ni contents, most of the Raman modes of our spinel nanostructures appeared at relatively lower wavenumbers in comparison to their reported positions for corresponding compositions (Table 3). Such a lower wavenumber shift of the Raman bands might be due to heating of the samples by laser exposure during measurement, as has also been observed by Windisch et al. for their $NiCo_2O_4$ thin films.[47] The Raman bands appeared at lower energy values for intermediate nickel content samples, i.e., for Ni:Co ratios of 1:2 and 1:3 (i.e., compositions closer to the stoichiometric $NiCo_2O_4$), due to fewer Co^{3+}/Ni^{3+} (i.e., Co^{3+} + Ni^{3+}) ions at O_h sites in their lattice (∼1 per formula unit). The remaining O_h sites in these two samples are occupied by Ni^{2+} ions. On the other hand, for the samples with Ni:Co ratios of 1:1 and 1:4, the number of Co^{3+}/Ni^{3+} ions at O_h sites is higher (∼1.5 and 1.4 per formula unit, respectively). Relatively higher energy positions of the O_h site-dependent Raman modes (i.e., ∼456, ∼504, and ∼645 cm^{-1}) in these samples are due to stronger bonding of the 3+ valence state ions with oxygen atoms of the lattice, as has been evidenced from their crystal field splitting (Δ) values presented in the Supporting Information. However, the position of the band appearing at ∼186 cm^{-1} corresponds to the tetrahedral sites containing either bivalent or trivalent cations,[48] which did not vary substantially (only 5 cm^{-1} in the present work) by changing the nickel mole fraction in the lattice. On the other hand, the relative intensity of the ∼186 cm^{-1} Raman band increased considerably for the sample with a Ni:Co ratio of 1:4, probably due to the presence of Co^{2+} ions at T_d sites. Furthermore, substitution of Co^{3+} by Ni^{2+} ions induces a charge imbalance in the Co_3O_4 lattice, which is compensated by the transformation of the direct spinel to an inverse spinel structure, where the O_h sites occupied by trivalent cations are substituted by divalent cations.

The sharp dispersion band appearing around 851 cm^{-1} (Figure 4) for all the samples corresponds to the carbonate groups.[34] We did not detect any Raman signal corresponding to NiO phase in the spinel nanostructures, which generally produces a broad signal around 510 cm^{-1}.[50] On the other hand, the commonly observed sharp and intense band appearing around 691 cm^{-1} (A_{1g} mode) in the Raman spectrum of Co_3O_4[46] was not revealed in the Raman spectra of our $Ni_xCo_{3-x}O_4$ nanoparticles, clearly indicating the absence of Co_3O_4 phase in them.

To study the effect of the Ni mole fraction on the magnetic behavior of the mixed oxide nanoparticles, their magnetization curves were recorded at different temperatures in a wide range of applied magnetic field. As can be observed in the $M-H$ curve recorded at 1.8 K (Figure 5), the Ni−Co mixed oxide nanoparticles with Ni:Co ratios of 1:1, 1:2, and 1:3 exhibit ferrimagnetic behavior with coercive field (H_c) of ∼1300 Oe. However, the sample with Ni:Co = 1:4 presents a superparamagnetic behavior, with a coercive field of only about 128 Oe. At 1.8 K, the saturation magnetization (M_s) of the mixed oxide nanoparticles varied following the order Ni:Co = 1:2 ≈ 1:3 < 1:1 < 1:4 (see Figure 5f). As there do not exist enough reports on the magnetization values of $Ni_xCo_{3-x}O_4$ nanostructures of different Ni mole fractions in the literature, we could not compare the M_s values of our nanostructures with literature values. However, as can be seen in Table S4, the

https://dx.doi.org/10.1021/acs.jpcc.0c03075
J. Phys. Chem. C 2020, 124, 18264−18274

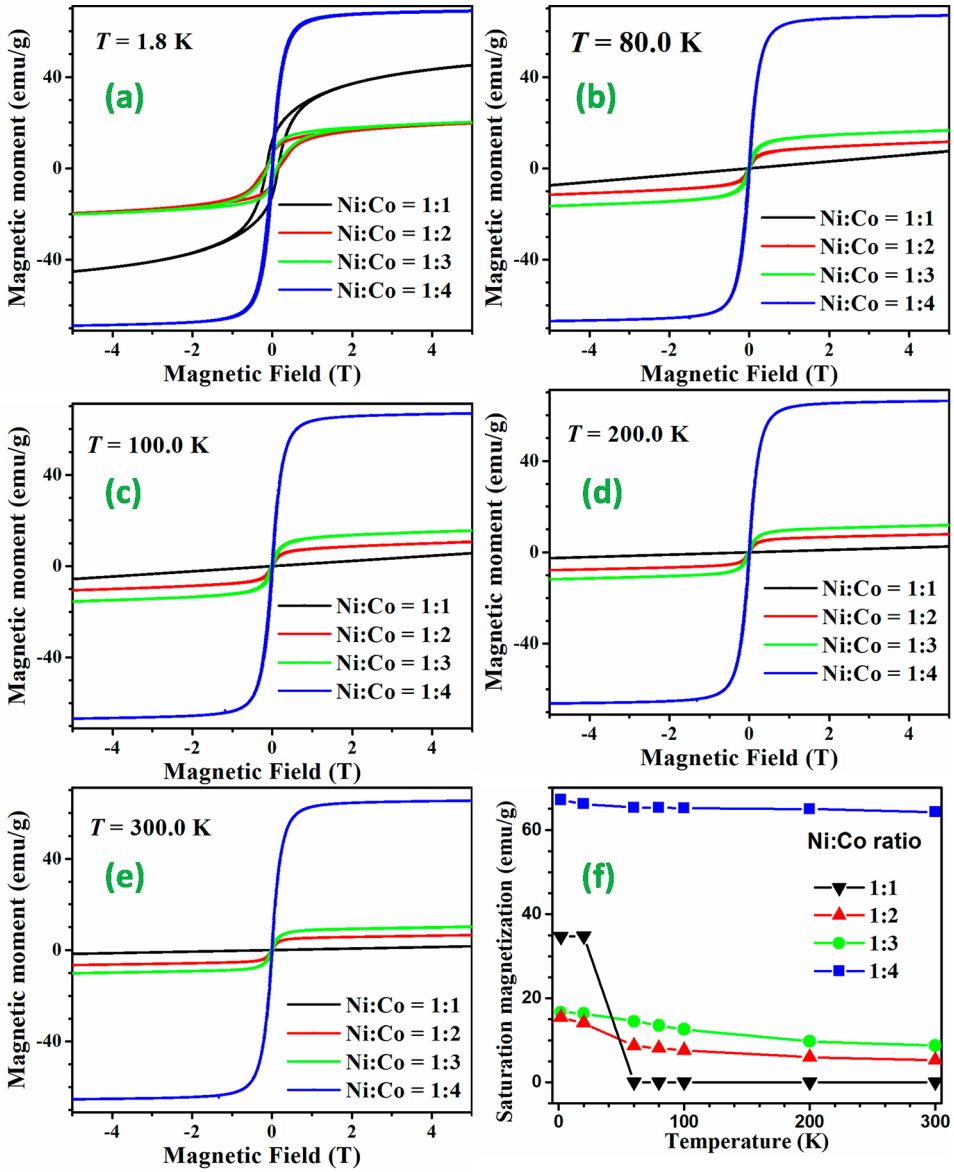

Figure 5. (a–e) Magnetization hysteresis and (f) saturation magnetization values of Ni–Co mixed oxide nanoparticles recorded at different temperatures. Values presented in (f) were obtained after subtraction of the paramagnetic component.

M_s value obtained at 1.8 K for our $NiCo_2O_4$ nanoparticles (Ni:Co = 1:2) is considerably low, although their room temperature M_s value remained among the highest reported in the literature.

Reported M_s values for $NiCo_2O_4$ nanostructures are included in Table S4. The lower low-temperature M_s value estimated for the $NiCo_2O_4$ nanostructures fabricated in the present work in comparison to the reported literature values is due to the presence of $Ni_{1-x}Co_xO$ impurity (with cubic NaCl-type structure). However, the room temperature M_s value of the sample is among the highest, even though the presence of carbon and metal carbonate impurities in the nanostructures might have reduced their M_s values to some extent. Note that the sample with lowest Ni content (Ni:Co = 1:4) revealed the highest M_s value (68.9 emu/g). At 80.0 K, while the sample with the lowest Ni content (Ni:Co = 1:4) still remained superparamagnetic with an almost unchanged M_s value, the M_s value of the nanoparticles with higher Ni contents reduced considerably, and their magnetic behavior changed from ferrimagnetic to paramagnetic. However, above 80.0 K, the magnetic behavior of the nanoparticles did not change significantly.

While the reduction in M_s for the mixed oxide nanoparticles at higher temperature is due to partial randomization of spin orientation at higher thermal energies, change in saturation magnetization (M_s) with increasing Ni content in the nanoparticles is due to replacement of $Co^{2+,3+}$ ions by $Ni^{2+,3+}$ ions. The observed variation of the M_s value with Ni fraction variation in the Ni–Co mixed oxides can be easily understood from Table 5, where the estimated net magnetic moments for the samples are compared with corresponding experimental values for some proposed cation distributions. Rows in italics in Table 5 indicate the most probable cation distributions based on the obtained spectroscopic and magnetic results of the fabricated mixed oxide nanostructures. As can be noticed in Table 5, the estimated and experimental net magnetic moments of the samples with Ni:Co = 1:2 and 1:3 differ significantly from the magnetic moments of other samples as

https://dx.doi.org/10.1021/acs.jpcc.0c03075
J. Phys. Chem. C 2020, 124, 18264–18274

these two samples contain $Ni_{1-x}Co_xO$ byproduct, which exhibits an antiferromagnetic order. The reported experimental magnetic moments for pure $NiCo_2O_4$ (Ni:Co = 1:2) are 2 μ_B (46.45 emu/g)[6] and 1.5 μ_B (34.84 emu/g),[51] which are close to the value estimated for the sample we prepared with Ni:Co = 1:2. As can be noticed, the λ values for the samples with Ni:Co ratios of 1:1 and 1:4 are 0.5 and 0.6, respectively. The result is in complete agreement with our claim (see Raman results discussion) about a certain degree of direct spinel structure for the mixed oxide nanostructures prepared with Ni:Co ratios of 1:1 and 1:4. In fact, the presence of both Ni^{2+} and Ni^{3+} ions in Ni−Co oxides has been demonstrated by Bitla et al.[6] through X-ray absorption spectroscopy (XAS).

To interpret the magnetic behavior of the sample containing the lowest nickel fraction (Ni:Co = 1:4), it is necessary to recall the magnetic ordering of the Co_3O_4 phase, alternatively represented as $Co^{2+}[Co^{3+}_2]O^{2-}_4$. In this oxide, the Co^{3+} cations are located at O_h sites and their net magnetic moment is 0 due to the electronic configuration $t_{2g}^6e_g^0$. Since the e_g state is ∼20 760 cm^{-1} higher in energy than the t_{2g} state, all six electrons of the valence shell in the Co^{3+} ion remain in the three t_{2g} states.[43] On the other hand, the eight Co^{2+} ions in one unit cell are located at T_d sites and they form an antiferromagnetic ordering of spin (Néel temperature ∼40 K).[52] On incorporating Ni^{2+} ions in the $Co^{2+}[Co^{3+}_2]O_4$ lattice, phases such as $Co^{3+}_{0.6}Co^{2+}_{0.4}[Ni^{2+}_{0.6}Co^{3+}_{1.4}]O_4$ can be formed (Figure 6). The net magnetic moment of this phase is ∼2.88

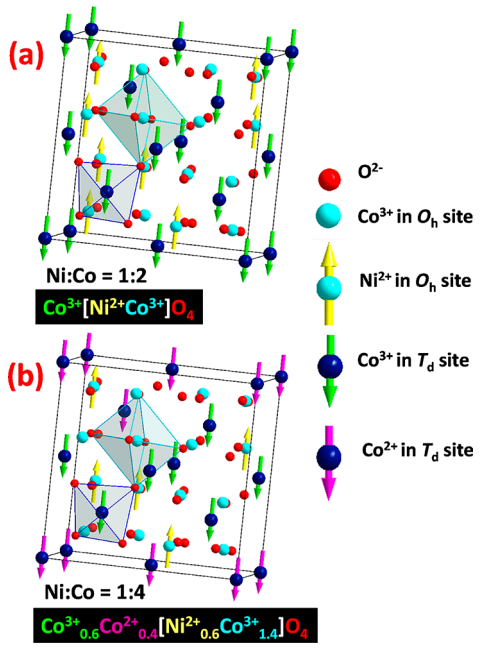

Figure 6. Schematic of cubic spinel lattice showing spin alignment of cations demonstrating the change in magnetic properties of the samples with Ni:Co ratios (a) 1:2 and (b) 1:4 (b). While the Ni^{2+} ions at O_h sites have spin up, the Co^{2+} and Co^{3+} ions at T_d sites have spin down.

μ_B or ∼66.86 emu/g (last row of Table 5). As can be noted in Table 5, the experimentally determined magnetic moment (2.96 μ_B) of the mixed oxide sample with Ni:Co = 1:4 is close to this value. A small discrepancy between the experimental and estimated magnetic moments of the sample probably occurred due to a small error in the calculation of effective magnetic moment (μ_{eff}) of the cations (Table S1) used for the estimation of the μ_{eff} of the spinel (Table 5). The electronic configurations assumed for Co^{3+} ions at O_h and T_d sites for these two phases are $t_{2g}^6e_g^0$ and $e_g^3t_{2g}^3$, respectively. In other words, the magnetization of the sample with Ni:Co = 1:4 might be due to the contributions of Co^{2+} and Co^{3+} ions at T_d sites and Ni^{2+} ions at O_h sites rather than the Co^{3+} ions at O_h sites.

While the magnetization curve of the sample with the lowest Ni content (Ni:Co = 1:4) indicates its soft-magnetic behavior, the sample containing the highest Ni content (Ni:Co = 1:1) revealed paramagnetic behavior above 20 K. The ferrimagnetic to paramagnetic transformation of the sample (Ni:Co = 1:1) above 20 K could be due to weak magnetic exchange interaction (J) among the $Ni^{2+,3+}$ cations located at O_h sites, which can be easily overcome by the thermal energy (k_BT). It is worth mentioning that the magnetization of the sample with a Ni:Co ratio of 1:1 might be originated exclusively from Ni^{2+} and $Co^{2+,3+}$ cations bonded to CO_3^{2-} anions. The presence of NiO nanoparticles formed by oxidation of segregated Ni clusters in the sample is ruled out, as the reported M_s value for NiO NPs (∼3 nm size) is only 15 emu/g (0.20 μ_B) at 5 K,[53] and also there is no evidence of NiO formation in the XRD pattern of the sample.

Figure 6 presents the schematic of the cubic spinel lattice with spin alignment of the cations to demonstrate the change in magnetic properties of the samples with Ni:Co ratios of 1:2 and 1:4. Note that while the lattice presented in Figure 6a corresponds to an inverse spinel structure (λ = 1.0), the lattice in Figure 6b has a partially inverse (λ = 0.6) spinel structure. In magnetic materials of spinel structure, the spins of the cations located at both O_h and T_d sites have parallel alignment among themselves. However, there is antiparallel alignment between the spins of cations at T_d sites and the spins of the cations at O_h sites.[54] Consequently, the net magnetization in the lattice is the difference between the magnetization generated by the cations at T_d sites and the cations at O_h sites. Considering that the only species in O_h sites that has spin is Ni^{2+}, the mentioned difference is largest when the amount of nickel is lowest (i.e., when the Ni:Co ratio is 1:4).

The zero field cooling and field cooling (ZFC and FC, respectively) curves of the fabricated nanoparticles are presented in Figure 7. For the ZFC measurements, all the samples were cooled from room temperature to 1.8 K (at 1 K/min) without application of any magnetic field, while for the FC measurements the samples were cooled under a constant magnetic field of 100 Oe. The ZFC−FC curves of the mixed oxide nanoparticles with a Ni mole fraction lower than 1.0 did not overlap below 300 K, which demonstrates that these three samples present ferrimagnetic/superparamagnetic ordering in the 1.8−300 K range. As can be observed in the ZFC profiles of the mixed oxide nanoparticles, the blocking temperature (T_B) varies with their Ni contents. The appearance of well-defined T_B in the Ni−Co mixed oxide samples indicates their transition from ferrimagnetic to superparamagnetic state. The mixed oxides with Ni:Co ratios of 1:2 and 1:3 revealed T_B's at 50.2 and 53.8 K, respectively, which correspond to the $Ni_xCo_{3-x}O_4$ phases of spinel type structure. However, Zhu et al. detected a transition temperature at 51 K in their $NiCo_2O_4$/NiO composite and attributed it to its spin glass state.[55] While the samples with Ni:Co molar ratios of 1:2 and 1:3 revealed their superparamagnetic behavior above T_B, below T_B they behaved as ferrimagnetic. The ZFC curve of the sample with Ni:Co = 1:2 revealed an additional sharp peak at 10.7 K, which

https://dx.doi.org/10.1021/acs.jpcc.0c03075
J. Phys. Chem. C 2020, 124, 18264−18274

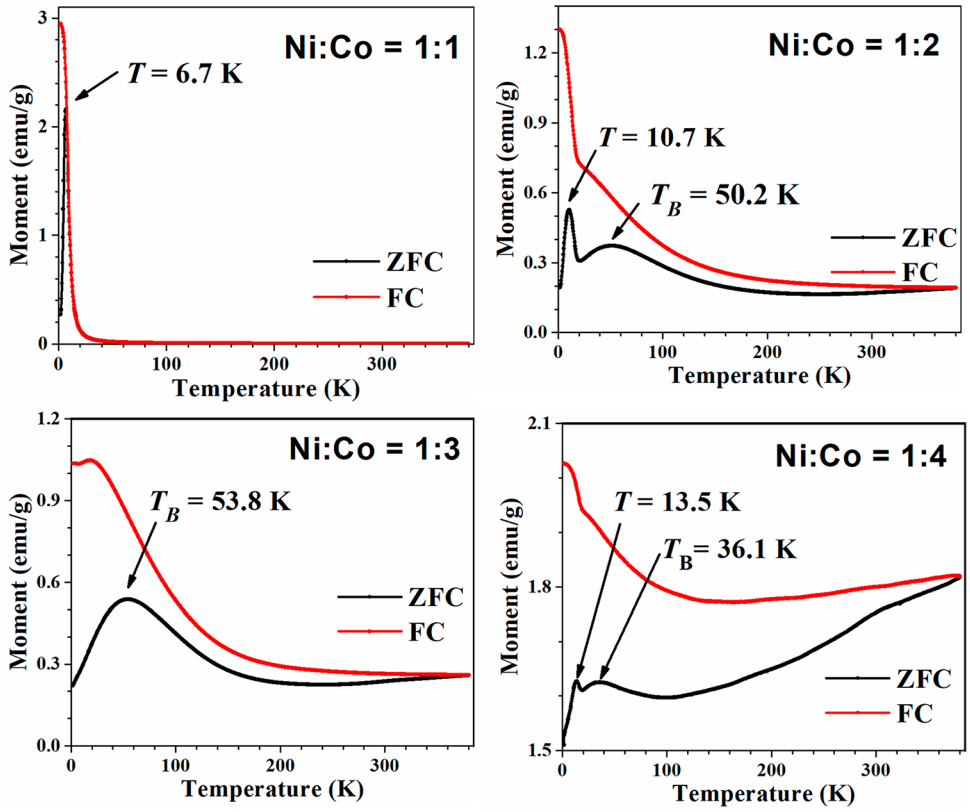

Figure 7. Field cooling (FC) and zero field cooling (ZFC) curves for Ni−Co oxide nanoparticles prepared with different Ni:Co molar ratios, recorded under 100 Oe applied magnetic field.

can be attributed to metal carbonate impurities. In fact, such an additional peak in the ZFC curve has been observed by Liu et al. for their porous $NiCo_2O_4$ nanosheets containing $Co_2CO_3(OH)_2$ and $Ni_2CO_3(OH)_2$ impurities.[56] On the other hand, the ZFC and FC curves of the sample with Ni:Co = 1:1 bifurcate at 6.7 K, which corresponds to its Curie temperature (T_C), at which the magnetic behavior changes from ferromagnetic to paramagnetic.

Finally, the ZFC curve of the sample with Ni:Co = 1:4 revealed a low-intensity peak located at 13.5 K, associated with traces of metal carbonate impurities. The ZFC−FC curves of the sample further demonstrate the superparamagnetic behavior of the sample, with T_C above 370 K. As has been observed in the $M-H$ curve in Figure 5, the sample with Ni:Co = 1:4 has a high M_s value (66.3 emu/g at 300 K). To the best of our knowledge, this is the highest M_s value reported for nickel cobaltite ($Ni_xCo_{3-x}O_4$). As can be noticed from the results presented above, the mixed oxide nanostructures prepared with nominal Ni:Co = 1:4 is quite unique among all the nanostructures fabricated in this work. While the structural phase and magnetic behavior of the mixed oxide nanostructures varied gradually with the variation of Ni content in the $1.0 \leq x \geq 0.33$ mole fraction range, both structural and magnetic phases of the nanostructures prepared at $x = 0.25$ (Ni:Co = 1:4) are quite different from those of the other nanostructures. Such unique structural and magnetic behaviors of the Ni−Co mixed oxide nanostructures are attributed to the distinct distribution of $Co^{2+,3+}$ ions at T_d sites and Ni^{2+} ions at O_h sites in their lattice. The {$Co^{2+,3+}$ at T_d sites}/{Ni^{2+} at O_h sites} ratio for this sample is the highest (1.66) among the four samples. While the magnetic behaviors of the mixed oxide nanostructures prepared with Ni:Co = 1:2 and 1:3 molar ratios indicate their potential for technological applications such as in electrochemical devices, the room temperature superparamagnetic nature with high M_s and low H_c of the nanostructures fabricated at the Ni:Co = 1:4 ratio clearly highlight their potential in electrical devices (e.g., transformer cores),[57] biomedical applications such as in hyperthermia,[58] and targeted drug delivery[59] for cancer treatments. Although the presence of undesired carbon in these spinel nanostructures is less probable to affect their biomedical applications, it may affect their performance in electrochemical devices.

4. CONCLUSIONS

In summary, Ni−Co mixed oxide nanoparticles of 17−40 nm size range and different Ni mole fractions could be fabricated successfully using a facile, low temperature glycol-mediated sol−gel process. Incorporation of Ni in the Co_3O_4 lattice is seen to invert its direct spinel type crystal structure to partially inverse spinel structure due to the substitution of Co ions by Ni ions in octahedral (O_h) sites. Incorporation of Ni in higher concentration (e.g., Ni:Co = 1:2 and 1:3) induces the formation of secondary phase $Ni_{1-x}Co_xO$ of cubic NaCl-type structure, which reduces the saturation magnetization M_s of the mixed oxide nanostructures. On the other hand, incorporation of Ni in very low concentration (e.g., Ni:Co = 1:4) generates nanoparticles of smaller sizes, converts their inverse spinel structure to partially inverse spinel structure, and induces superparamagnetism due to very low magnetocrystalline anisotropy. Due to the soft-magnetic nature, high M_s, high T_C, and low H_c of the mixed oxide nanostructures fabricated with Ni:Co = 1:4, they have a great potential to be utilized for

https://dx.doi.org/10.1021/acs.jpcc.0c03075
J. Phys. Chem. C 2020, 124, 18264−18274

biomedical applications such as magnetic hyperthermia and targeted drug delivery for cancer treatment.

■ ASSOCIATED CONTENT

Supporting Information

The Supporting Information is available free of charge at https://pubs.acs.org/doi/10.1021/acs.jpcc.0c03075.

Estimation of effective magnetic moments (μ_{eff}) for $Co^{2+,3+}$ and $Ni^{2+,3+}$ ions in tetrahedral and octahedral sites; reported Shannon ionic radii (angstroms) and estimated magnetic moments {spin-only (μ_{so}), effective (μ_{eff})} for $Co^{2+,3+}$ and $Ni^{2+,3+}$ ions in tetrahedral and octahedral sites; reported spin−orbit coupling coefficients (λ) and crystal field splitting (Δ) for $Co^{2+,3+}$ and $Ni^{2+,3+}$ ions (PDF)

■ AUTHOR INFORMATION

Corresponding Author

Umapada Pal − *Instituto de Física, Benemérita Universidad Autónoma de Puebla, Puebla 72570, Mexico;* orcid.org/0000-0002-5665-106X; Phone: +52 (222) 2295610; Email: upal@ifuap.buap.mx

Authors

Jesús Alberto Ramos Ramón − *Instituto de Física, Benemérita Universidad Autónoma de Puebla, Puebla 72570, Mexico*

Jose Luis Ortiz-Quiñonez − *Instituto de Física, Benemérita Universidad Autónoma de Puebla, Puebla 72570, Mexico*

Apurba Ray − *Department of Instrumentation Science, Jadavpur University, Kolkata 700032, India*

Sachindranath Das − *Department of Instrumentation Science, Jadavpur University, Kolkata 700032, India;* orcid.org/0000-0002-6938-6701

Complete contact information is available at: https://pubs.acs.org/10.1021/acs.jpcc.0c03075

Notes

The authors declare no competing financial interest.

■ ACKNOWLEDGMENTS

This work has been partially supported by CONACyT (Grant No. INFR-2014-02-23053, A1-S-26720), VIEP—BUAP (Grant No. VIEP/EXC/2018), Mexico, and Science and Engineering Research Board, Department of Science and Technology, Government of India, through the "Core Research Grant" (File No. CRG/2019/001575 PI-S Das). J.L.O.-Q. thanks CONACyT for providing a postdoctoral fellowship.

■ REFERENCES

(1) Lu, X.; Huang, X.; Xie, S.; Zhai, T.; Wang, C.; Zhang, P.; Yu, M.; Li, W.; Liang, C.; Tong, Y. Controllable Synthesis of Porous Nickel−Cobalt Oxide Nanosheets for Supercapacitors. *J. Mater. Chem.* **2012**, *22*, 13357−13364.

(2) Wang, Q.; Liu, B.; Wang, X.; Ran, S.; Wang, L.; Chen, D.; Shen, G. Morphology Evolution of Urchin-like $NiCo_2O_4$ Nanostructures and their Applications as Psuedocapacitors and Photoelectrochemical Cells. *J. Mater. Chem.* **2012**, *22*, 21647−21653.

(3) Li, Y.; Hasin, P.; Wu, Y. $Ni_xCo_{3-x}O_4$ Nanowire Arrays for Electrocatalytic Oxygen Evolution. *Adv. Mater.* **2010**, *22*, 1926−1929.

(4) Li, Q.; Zeng, L.; Wang, J.; Tang, D.; Liu, B.; Chen, G.; Wei, M. Magnetic Mesoporous Organic-Inorganic $NiCo_2O_4$ Hybrid Nanomaterials for Electrochemical Immunosensors. *ACS Appl. Mater. Interfaces* **2011**, *3*, 1366−1373.

(5) Kale, S. N.; Jadhav, A. D.; Verma, S.; Koppikar, S. J.; Kaul-Ghanekar, R.; Dhole, S. D.; Ogale, S. B. Characterization of Biocompatible $NiCo_2O_4$ Nanoparticles for Applications in Hyperthermia and Drug Delivery. *Nanomedicine* **2012**, *8*, 452−459.

(6) Bitla, Y.; Chin, Y.-Y.; Lin, J.-C.; Van, C. N.; Liu, R.; Zhu, Y.; Liu, H.-J.; Zhan, Q.; Lin, H.-J.; Chen, C.-T.; et al. Origin of Metallic Behavior in $NiCo_2O_4$ Ferrimagnet. *Sci. Rep.* **2015**, *5*, 15201.

(7) Iliev, M. N.; Silwal, P.; Loukya, B.; Datta, R.; Kim, D. H.; Todorov, N. D.; Pachauri, N.; Gupta, A. Raman Studies of Cation Distribution and Thermal Stability of Epitaxial Spinel $NiCo_2O_4$ Films. *J. Appl. Phys.* **2013**, *114*, 033514.

(8) Marco, J. F.; Gancedo, J. R.; Gracia, M.; Gautier, J. L.; Ríos, E. I.; Palmer, H. M.; Greaves, C.; Berry, F. J. Cation Distribution and Magnetic Structure of the Ferrimagnetic Spinel $NiCo_2O_4$. *J. Mater. Chem.* **2001**, *11*, 3087−3093.

(9) Pandey, P.; Bitla, Y.; Zschornak, M.; Wang, M.; Xu, C.; Grenzer, J.; Meyer, D. C.; Chin, Y. Y.; Lin, H. J.; Chen, C. T.; et al. Enhancing the Magnetic Moment of Ferrimagnetic $NiCo_2O_4$ Via Ion Irradiation Driven Oxygen Vacancies. *APL Mater.* **2018**, *6*, 066109.

(10) Verma, S.; Kumar, A.; Pravarthana, D.; Deshpande, A.; Ogale, S. B.; Yusuf, S. M. Off-Stoichiometric Nickel Cobaltite Nanoparticles: Thermal Stability, Magnetization, and Neutron Diffraction Studies. *J. Phys. Chem. C* **2014**, *118*, 16246−16254.

(11) Cabo, M.; Pellicer, E.; Rossinyol, E.; Castell, O.; Suriñach, S.; Baró, M. D. Mesoporous $NiCo_2O_4$ Spinel: Influence of Calcination Temperature over Phase Purity and Thermal Stability. *Cryst. Growth Des.* **2009**, *9*, 4814−4821.

(12) Nayak, P.; Sahoo, M.; Nayak, S. K. Urchin-like $NiCo_2O_4$ Microsphere by Hydrothermal Route: Structural, Electrochemical, Optical and Magnetic Properties. *Ceram. Int.* **2020**, *46*, 3818−3826.

(13) Yang, X.; Yu, X.; Yang, Q.; Zhao, D.; Zhang, K.; Yao, J.; Li, G.; Zhou, H.; Zuo, X. Controllable Synthesis and Magnetic Properties of Hydrothermally Synthesized $NiCo_2O_4$ Nano-spheres. *Ceram. Int.* **2017**, *43*, 8585−8589.

(14) Umeshbabu, E.; Rajeshkhanna, G.; Justin, P.; Rao, G. R. Magnetic, Optical and Electrocatalytic Properties of Urchin and Sheaf-like $NiCo_2O_4$ Nanostructures. *Mater. Chem. Phys.* **2015**, *165*, 235−244.

(15) Nakate, U. T.; Kale, S. N. Microwave Assisted Synthesis and Characterizations of $NiCo_2O_4$ Nanoplates and Electrical, Magnetic Properties. *Mater. Today Proc.* **2016**, *3*, 1992−1998.

(16) Kumar, B. S.; Dhanasekhar, C.; Venimadhav, A.; Kalpathy, S. K.; Anandhan, S. Pyrolysis-controlled Synthesis and Magnetic Properties of Sol−Gel Electrospun Nickel Cobaltite Nanostructures. *J. Sol-Gel Sci. Technol.* **2018**, *86*, 664−674.

(17) Wang, P.; Wu, C.; Zhen, C.; Li, G.; Pan, C.; Ma, L.; Hou, D. Modulation of the Structure and Magnetic Properties of the $Ni_{1-x}Co_{2-y}O_4$ Powders by Hydrothermal Temperature. *Phys. B* **2019**, *561*, 147−154.

(18) Dubal, D. P.; Gomez-Romero, P.; Sankapal, B. R.; Holze, R. Nickel Cobaltite as an Emerging Material for Supercapacitors: An Overview. *Nano Energy* **2015**, *11*, 377−399.

(19) Zhang, L.; Shi, D.; Liu, T.; Jaroniec, M.; Yu, J. Nickel-based Materials for Supercapacitors. *Mater. Today* **2019**, *25*, 35−65.

(20) Guo, X.; Chen, C.; Zhang, Y.; Xu, Y.; Pang, H. The Application of Transition Metal Cobaltites in Electrochemistry. *Energy Storage Mater.* **2019**, *23*, 439−465.

(21) Catalan, B. G.; Scott, J. F. Physics and Applications of Bismuth Ferrite. *Adv. Mater.* **2009**, *21*, 2463−2485.

(22) Roy, P.; Hoque, S. M.; Liba, S. I.; Choudhury, S. Investigation of Various Magnetic Features of Spinel type Cobalt Ferrite ($CoFe_2O_4$) Nanoparticles Tuned by Annealing Temperature. *AIP Adv.* **2018**, *8*, 105124.

(23) Windisch, C. F.; Exarhos, G. J.; Owings, R. R. Vibrational Spectroscopic Study of the Site Occupancy Distribution of Cations in Nickel Cobalt Oxides. *J. Appl. Phys.* **2004**, *95*, 5435−5442.

(24) Marco, J. F.; Gancedo, J. R.; Gracia, M.; Gautier, J. L.; Ríos, E.; Berry, F. J. Characterization of the Nickel Cobaltite, $NiCo_2O_4$, Prepared by Several Methods: An XRD, XANES, EXAFS, and XPS study. *J. Solid State Chem.* **2000**, *153*, 74−81.
(25) Das, B.; Reddy, M. V.; Chowdari, B. V. R. X-ray Absorption Spectroscopy and Energy Storage of Ni-Doped Cobalt Nitride, $(Ni_{0.33}Co_{0.67})N$, Prepared by a Simple Synthesis Route. *Nanoscale* **2013**, *5*, 1961−1966.
(26) Liu, Z.-Q.; Xiao, K.; Xu, Q.-Z.; Li, N.; Su, Y.-Z.; Wang, H.-J.; Chen, S. Fabrication of Hierarchical Flower-like Super-Structures Consisting of Porous $NiCo_2O_4$ Nanosheets and their Electrochemical and Magnetic Properties. *RSC Adv.* **2013**, *3*, 4372−4380.
(27) Lu, Z.; Xia, G.; Templeton, J. D.; Li, X.; Nie, Z.; Yang, Z.; Stevenson, J. W. Development of $Ni_{1-x}Co_xO$ as the Cathode/Interconnect Contact for Solid Oxide Fuel Cells. *Electrochem. Commun.* **2011**, *13*, 642−645.
(28) Khalid, S.; Cao, C.; Wang, L.; Zhu, Y. Microwave Assisted Synthesis of Porous $NiCo_2O_4$ Microspheres: Application as High Performance Asymmetric and Symmetric Supercapacitors with Large Areal Capacitance. *Sci. Rep.* **2016**, *6*, 22699.
(29) Zhan, J.; Cai, M.; Zhang, C.; Wang, C. Synthesis of Mesoporous $NiCo_2O_4$ Fibers and their Electrocatalytic Activity on Direct Oxidation of Ethanol in Alkaline Media. *Electrochim. Acta* **2015**, *154*, 70−76.
(30) Ding, R.; Qi, L.; Jia, M.; Wang, H. Facile Synthesis of Mesoporous Spinel $NiCo_2O_4$ Nanostructures as Highly Efficient Electrocatalysts for Urea Electro-Oxidation. *Nanoscale* **2014**, *6*, 1369−1376.
(31) Ray, A.; Roy, A.; Sadhukhan, P.; Chowdhury, S. R.; Maji, P.; Bhattachrya, S. K.; Das, S. Electrochemical Properties of TiO_2-V_2O_5 Nanocomposites as a High Performance Supercapacitors Electrode Material. *Appl. Surf. Sci.* **2018**, *443*, 581−591.
(32) Ray, A.; Roy, A.; Bhattacharjee, S.; Jana, S.; Ghosh, C. K.; Sinha, C.; Das, S. Correlation between the Dielectric and Electrochemical Properties of TiO_2-V_2O_5 Nanocomposite for Energy Storage Application. *Electrochim. Acta* **2018**, *266*, 404−413.
(33) Mohamed, M. A.; Halawy, S. A.; Ebrahim, M. M. Non-isothermal Decomposition of Nickel Acetate Tetrahydrate. *J. Anal. Appl. Pyrolysis* **1993**, *27*, 109−110.
(34) Fujita, J.; Martell, A. E.; Nakamoto, K. Infrared Spectra of Metal Chelate Compounds. VIII. Infrared Spectra of Co(III) Carbonato Complexes. *J. Chem. Phys.* **1962**, *36*, 339−345.
(35) Hu, C.-C.; Hsu, C.-T.; Chang, K.-H.; Hsu, H.-Y. Microwave-assisted Hydrothermal Annealing of Binary Ni−Co Oxy-Hydroxides for Asymmetric Supercapacitors. *J. Power Sources* **2013**, *238*, 180−189.
(36) Dubal, D. P.; Jagadale, A. D.; Patil, S. V.; Lokhande, C. D. Simple Route for the Synthesis of Supercapacitive Co−Ni Mixed Hydroxide Thin Films. *Mater. Res. Bull.* **2012**, *47*, 1239−1245.
(37) Morales Flores, N.; Pal, U.; Galeazzi, R.; Sandoval, A. Effects of Morphology, Surface Area, and Defect Content on the Photocatalytic Dye Degradation Performance of ZnO Nanostructures. *RSC Adv.* **2014**, *4*, 41099−41110.
(38) Dileep, K.; Loukya, B.; Silwal, P.; Gupta, A.; Datta, R. Probing Optical Band Gaps at Nanoscale from Tetrahedral Cation Vacancy Defects and Variation of Cation Ordering in $NiCo_2O_4$ Epitaxial Thin Films. *J. Phys. D: Appl. Phys.* **2014**, *47*, 405001.
(39) Shannon, R. D. Revised Effective Ionic Radii and Systematic Studies of Interatomic Distances in Halides and Chalcogenides. *Acta Crystallogr., Sect. A: Cryst. Phys., Diffr., Theor. Gen. Crystallogr.* **1976**, *32*, 751−767.
(40) Gourrier, L.; Deabate, S.; Michel, T.; Paillet, M.; Hermet, P.; Bantignies, J.; Henn, F. Characterization of Unusually Large "Pseudo-Single Crystal" of β-Nickel Hydroxide. *J. Phys. Chem. C* **2011**, *115*, 15067−15074.
(41) Johnston, C.; Graves, P. R. In Situ Raman Spectroscopy Study of the Nickel Oxyhydroxide Electrode (NOE) System. *Appl. Spectrosc.* **1990**, *44*, 105−114.
(42) Hall, D. S.; Lockwood, D. J.; Poirier, S.; Bock, C.; MacDougall, B. R. Raman and Infrared Spectroscopy of α and β Phases of Thin Nickel Hydroxide Films Electrochemically Formed on Nickel. *J. Phys. Chem. A* **2012**, *116*, 6771−6784.
(43) Huheey, J. E.; Keiter, E. A.; Richard, L. K. *Inorganic Chemistry: Principles of Structure and Reactivity*, 4th ed.; HarperCollins College Publishers: New York, 1993.
(44) Zhao, Q.; Yan, Z.; Chen, C.; Chen, J. Spinels: Controlled Preparation, Oxygen Reduction/Evolution Reaction Application, and Beyond. *Chem. Rev.* **2017**, *117*, 10121−10211.
(45) Liu, Y.; Ying, Y.; Fei, L.; Liu, Y.; Hu, Q.; Zhang, G.; Pang, S. Y.; Lu, W.; Mak, C. L.; Luo, X. Valence Engineering via Selective Atomic Substitution on Tetrahedral Sites in Spinel Oxide for Highly Enhanced Oxygen Evolution Catalysis. *J. Am. Chem. Soc.* **2019**, *141*, 8136−8145.
(46) Hadjiev, V. G.; Iliev, M. N.; Vergilov, I. V. The Raman Spectra of Co_3O_4. *J. Phys. C: Solid State Phys.* **1988**, *21*, L199−L201.
(47) Windisch, C. F., Jr.; Exarhos, G. J.; Sharma, S. K. Influence of Temperature and Electronic Disorder on the Raman Spectra of Nickel Cobalt Oxides. *J. Appl. Phys.* **2002**, *92*, 5572−5574.
(48) Allen, G. C.; Paul, M. Chemical Characterization of Transition Metal Spinel-Type Oxides by Infrared Spectroscopy. *Appl. Spectrosc.* **1995**, *49*, 451−458.
(49) Su, Y. Z.; Xu, Q. Z.; Chen, G. F.; Cheng, H.; Li, N.; Liu, Z. Q. One Dimensionally Spinel $NiCo_2O_4$ Nanowire Arrays: Facile Synthesis, Water Oxidation, and Magnetic Properties. *Electrochim. Acta* **2015**, *174*, 1216−1224.
(50) Mrabet, C.; Ben Amor, M.; Boukhachem, A.; Amlouk, M.; Manoubi, T. Physical Properties of La-doped NiO Sprayed Thin Films for Optoelectronic and Sensor Applications. *Ceram. Int.* **2016**, *42*, 5963−5978.
(51) Battle, P. D.; Cheetham, A. K.; Goodenough, J. B. A Neutron Diffraction Study of the Ferrimagnetic Spinel $NiCo_2O_4$. *Mater. Res. Bull.* **1979**, *14*, 1013−1024.
(52) Roth, W. L. The Magnetic Structure of Co_3O_4. *J. Phys. Chem. Solids* **1964**, *25*, 1−10.
(53) Ghosh, M.; Biswas, K.; Sundaresan, A.; Rao, C. N. R. MnO and NiO Nanoparticles: Synthesis and Magnetic Properties. *J. Mater. Chem.* **2006**, *16*, 106−111.
(54) Spaldin, N. A. *Magnetic Material: Fundamentals and Applications*, 2nd ed.; Cambridge University Press: New York, 2010.
(55) Zhu, C. M.; Wang, L. G.; Liu, F. C.; Kong, W. J. Exchange Bias Behaviors up to Room Temperature in $NiCo_2O_4$/NiO Nanoparticle System. *Ceram. Int.* **2019**, *45*, 9878−9883.
(56) Liu, Z. Q.; Xiao, K.; Xu, Q. Z.; Li, N.; Su, Y. Z.; Wang, H. J.; Chen, S. Fabrication of Hierarchical Flower-like Super-Structures Consisting of Porous $NiCo_2O_4$ Nanosheets and their Electrochemical and Magnetic Properties. *RSC Adv.* **2013**, *3*, 4372−4380.
(57) David, J. *Introduction to Magnetism and Magnetic Materials*, 3rd ed.; CRC Press/Taylor and Francis: Boca Raton, FL, 2015.
(58) Simeonidis, K.; Martinez-Boubeta, C.; Balcells, L.; Monty, C.; Stavropoulos, G.; Mitrakas, M.; Matsakidou, A.; Vourlias, G.; Angelakeris, M. Fe-based Nanoparticles as Tunable Magnetic Particle Hyperthermia Agents. *J. Appl. Phys.* **2013**, *114*, 103904.
(59) Uribe Madrid, S. I.; Pal, U.; Kang, Y. S.; Kim, J.; Kwon, H.; Kim, J. Fabrication of Fe_3O_4@mSiO_2 Core-shell Composite Nanoparticles for Drug Delivery Applications. *Nanoscale Res. Lett.* **2015**, *10*, 217.

https://dx.doi.org/10.1021/acs.jpcc.0c03075
J. Phys. Chem. C 2020, 124, 18264−18274